Article

A Cross-Machine Comparison of Shear-Wave Speed Measurements Using 2D Shear-Wave Elastography in the Normal Female Breast

Emma Harris [1,*], Ruchi Sinnatamby [2], Elizabeth O'Flynn [3], Anna M. Kirby [1] and Jeffrey C. Bamber [1]

1   The Institute of Cancer Research and Royal Marsden Hospital NHS Foundation Trust, Radiotherapy and Imaging, London SM2 5PT, UK; anna.kirby@doctors.org.uk (A.M.K.); jeff.bamber@icr.ac.uk (J.C.B.)
2   Cambridge University Hospitals NHS Foundation Trust, Cambridge CB2 0QQ, UK; ruchi.sinnatamby@addenbrookes.nhs.uk
3   St George's University Hospitals NHS Foundation Trust, Radiology, London SW17 0QT, UK; lizoflynn@doctors.org.uk
*   Correspondence: emma.harris@icr.ac.uk

Abstract: Quantitative measures of radiation-induced breast stiffness are required to support clinical studies of novel breast radiotherapy regimens and exploration of personalised therapy, however, variation between shear-wave elastography (SWE) machines may limit the usefulness of shear-wave speed (c_s) for this purpose. Mean c_s measured in four healthy volunteers' breasts and a phantom using 2D-SWE machines Acuson S2000 (Siemens Medical Solutions) and Aixplorer (Supersonic Imagine) were compared. Shear-wave speed was measured in the skin region, subcutaneous adipose tissue and parenchyma. c_s estimates were on average 2.3% greater when using the Aixplorer compared to S2000 in vitro. In vivo, c_s estimates were on average 43.7%, 36.3% and 49.9% significantly greater ($p << 0.01$) when using the Aixplorer compared to S2000, for skin region, subcutaneous adipose tissue and parenchyma, respectively. In conclusion, despite relatively small differences between machines observed in vitro, large differences in absolute measures of shear wave speed measured were observed in vivo, which may prevent pooling of cross-machine data in clinical studies of the breast.

Keywords: shear-wave elastography; shear-wave speed; radiation-induced breast toxicity; tissue stiffness; cross-machine comparison

1. Introduction

Breast-conserving surgical local excision, followed by radiotherapy (RT) to improve local control and survival, is a successful treatment for early breast cancer. Approximately 31,000 women receive adjuvant breast RT in the UK per year with local relapse rates as low as ~6% at 10 years [1]. Given that many women are now surviving decades beyond their breast cancer treatment, a priority now is to reduce the long-term side effects of radiotherapy to the breast. The overall cosmetic outcome has been shown to be an important factor influencing patient psychosocial morbidity after treatment [2]. Evaluation of novel RT regimens must weigh the positive outcomes (including local control, disease-free survival, and overall survival) against treatment-related toxicity and the impact on the patient's quality of life. Currently, morbidity-related endpoints are primarily derived from subjective measures of function, patient comfort and cosmesis, as evaluated by clinicians or patients, which can be subject to variation due to psychological and social factors [3,4]. Such variation may preclude the pooling of results from multiple clinical studies of radiotherapy [5], required to support studies of genetic predisposition to radiation toxicity [6]. Quantitative, reproducible measures of morbidity could remove these sources of variation allowing more objective assessment of treatment toxicity and facilitating exploration of personalised treatment.

Shear-wave elastography (SWE) has the potential to quantify tissue stiffness for the purpose of disease diagnosis, prognosis or staging, and to monitor the response of tissues to treatment [7–12]. SWE is expected to be able to quantify properties related to breast tissue stiffness using shear-wave speed c_s, which under a number of assumptions is related to Young's modulus (E) of the tissue using $E = 3\rho c_s^2$, where ρ is tissue density [10]. Absolute or relative measures of c_s or E may be useful. One such relative measure could be the spatial distribution of c_s, which can be compared with the radiation dose distribution delivered to the patient, potentially helping to further increase understanding of the relationship between dose and radiation-induced morbidity. Two-dimensional SWE (2D-SWE) which provides the spatial distribution, or map, of c_s may be used for this purpose. Here, we adopt the convention for describing different forms of elastography outlined in Bamber et al. [13].

In the context of large multi-centre clinical trials, required to provide the clinical evidence to change practice [1], measures of morbidity must be reproducible between centres. There is evidence to suggest that c_s estimates vary between machines provided by different vendors, transducer types and imaging depth [14–16]. This may detrimentally affect the application of SWE to the assessment of normal tissue toxicity because it is unlikely that the same SWE equipment will be available across different clinical centres.

Investigations that compare c_s estimates made with various machines, transducers and system settings have been largely limited to *in vitro* studies [17–19], albeit with some in the liver *in vivo* [20,21]. No study has compared c_s estimates between machines in normal breast tissues. The purpose of the current study was to compare absolute and relative measures of breast c_s between 2D-SWE machines *in vivo* to determine if these could be used as reliable metrics in planned cross-centre and cross-machine clinical studies of radiation-induced fibrosis. Previous work has shown that the skin thickens post radiotherapy [22,23] and other work has indicated that women with greater breast size are more likely to experience breast hardening [24,25]. Larger breast size is associated with a greater proportion of adipose tissue. It may therefore be important to measure hardening in component breast tissues, i.e., skin, adipose and breast parenchyma. It is expected that different breast tissues will have different c_s [26–28] and that these differences are consistent between machines. Previous studies of point SWE (pSWE) suggest that c_s estimates are influenced by transducer orientation with respect to Cooper's ligaments [28]. If 2D-SWE c_s estimates are similarly affected, care must be taken to reproduce transducer orientation across centres.

In this study, we investigate the difference in c_s measured using two machines that provide 2D-SWE, the Aixplorer® (Supersonic Imagine, Aix-en-Provence, France) and the Acuson S2000® (Siemens Healthcare GmbH, Erlangen, Germany). Both machines generate shear waves in tissue using an acoustic radiation force impulse (ARFI), which creates a local tissue displacement at the focus of the ARFI beam. This small displacement of tissue generates shear waves that emanate from the focus. Although the approach to measuring c_s is similar there may be technical differences that lead to a variation in the value of c_s measured. For example, the Acuson builds up a 2D image by focusing the ARFI beam at multiple lateral locations at multiple depths. The shear waves are tracked using multiple tracking beams [13,29]. The Aixplorer uses a different approach, sweeping the ARFI focus over the depth of imaging faster than the speed of the shear waves, generating a cone-shaped shear wave, known as a Mach cone. This scanner tracks the propagation of the shear wave using ultrafast plane wave imaging, allowing the shear waves to be tracked in 2D [30]. Furthermore, each machine uses proprietary software to generate values of c_s using the tracking data. Consequently, differences in how the displayed value of c_s is calculated may also exist.

Variation between absolute measures of mean c_s values was investigated in different regions of the breast, specifically, the skin region, subcutaneous adipose tissue and, where it could be clearly differentiated, breast parenchyma. Relative measures investigated included tissue c_s ratio, the ratio of c_s, in pairs of the above tissue types and the anisotropy ratio, the ratio of c_s estimates acquired in transducer orientations that were radial and anti-radial with respect to the nipple.

2. Materials and Methods

2.1. Machines and Machine Settings

Cross-centre and cross-machine shear-wave speed (c_s) measurements were performed on an ultrasound elasticity phantom and four healthy female volunteers at two centres, the Royal Marsden National Health Service (NHS) Foundation Trust (RM) and Cambridge University Hospitals NHS Foundation Trust (CUH), on the same day. At RM, the Aixplorer® was used with an L10-2 linear probe and at CUH the Acuson S2000® with Virtual Touch Imaging Quantification (VTIQ®) technology and a 9L4 linear probe was used. Both machines produce a 2D elastogram, i.e., a map of c_s. The machine settings for the Aixplorer for B-Mode imaging were "Gen/Med", dynamic range = 61 dB, image persistence = medium, speed of sound = 1540 ms^{-1}, transmit frequency = 5 MHz and, for shear-wave elastography (SWE) mode, Penetration = Med, SWE map persistence level = high, Smoothing = 5 and G = 70%. At CUH, the S2000 settings for B-mode imaging were F = 9 MHz, dynamic range = 65 dB, speed of sound = 1540 m/s, persistence setting = 3. A maximum elastogram depth of 3.5 cm was used for both machines.

2.2. In Vitro Measurements

A tissue-mimicking phantom (Model 049 Elasticity QA Phantom, Computerized Imaging Reference Systems Inc. (CIRS), Norfolk, VA, USA) was used to obtain c_s estimates. The phantom was made of Zerdine®polymer and contained two groups of four spherical inclusions of four different elastic moduli different to the elastic modulus of the background material; one group was placed at a depth of 15 mm and the other at a depth of 35 mm, the former group was used in this study.

Three independent observers acquired shear-wave elastograms and c_s estimates from the four shallow inclusions (depth = 1.5 cm, diameter = 1.0 cm) and background material with both machines; deeper inclusions were too deep to fully visualise in SWE mode using the linear transducers used in the current study, which are designed for breast examinations. To determine Aixplorer c_s estimates within the inclusions, circular regions of interest (ROIs), called Q-Boxes, with a diameter of 1.0 cm were positioned over each inclusion and c_s estimates were recorded. The S2000 c_s estimates were acquired using nine 1.5 mm × 1.5 mm square (fixed by the manufacturer) ROIs positioned randomly within each inclusion and within the background material and c_s estimates were recorded. For both machines, all ROIs were positioned using the B-mode image, except for Aixplorer when artefacts were excluded and the elastogram was used to indicate the position of the artefacts. The artefacts are discussed in more detail in Section 2.4. Observers independently performed measurements three times and were blinded to the results of other observers.

2.3. In Vivo Imaging

Four healthy female volunteers with no history of breast malignancy were recruited for this study. The Surrey and South East Coast National Health Service Research Ethics Committee approved the study and informed consent was obtained from all the volunteers prior to scanning. Volunteers were aged 60, 38, 28 and 25 years on the date of scanning. A single consultant breast radiologist (RS at CUH, or EO at RM) acquired elastograms of the breast at each centre. Prior to acquiring data for analysis, radiologists practised acquiring elastograms without precompression, which may produce an overestimation of c_s and introduce SWE elastogram artefacts *in vivo* [31]. To avoid precompression, copious amounts of ultrasonic gel were used to create a stand-off. Volunteers were asked to hold their breath to make it easier to maintain this stand-off during each image acquisition and reduce the likelihood of motion artefacts.

Images were obtained first with the Aixplorer at RM, after which volunteers travelled to CUH and the imaging was repeated with the S2000. There was an average of six hours between scanning at the two centres. Eight images were acquired from each breast with the transducer in radial and anti-radial transducer orientations, as explained by Figure 1. The transducer positions employed at RM were marked using a surgical marker pen to

enable interrogation of the same regions of tissue at CUH. Volunteers were scanned supine with their arm raised behind their head. B-mode images and elastograms were acquired using the technique described above.
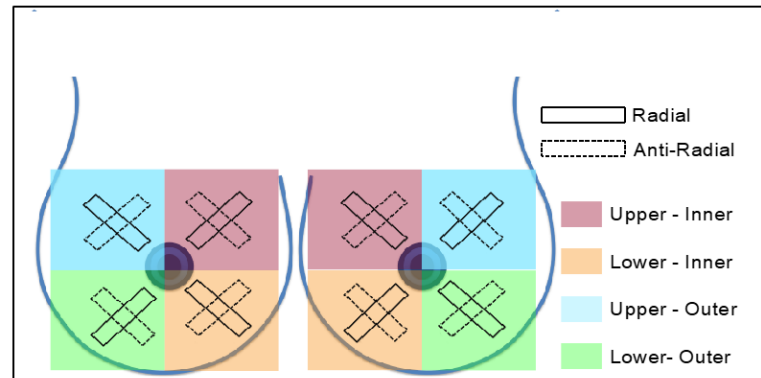

Figure 1. Schematic of transducer positions used to obtain shear-wave speed (c_s) estimates from the breast. Eight B-mode image and elastogram pairs were acquired from each breast.

2.4. Shear-Wave Speed Estimates

The S2000 generated a shear-wave speed grayscale elastogram adjacent to the B-mode image. See Figure 2a. A radiologist (RS) used the B-mode image to identify skin, adipose and parenchyma. Six ROIs were placed on each tissue type on the B-mode image. The S2000 provided on-screen annotations showing the position of each region of interest (ROI) in both the B-mode and the elastograms, and the mean c_s within the ROI.
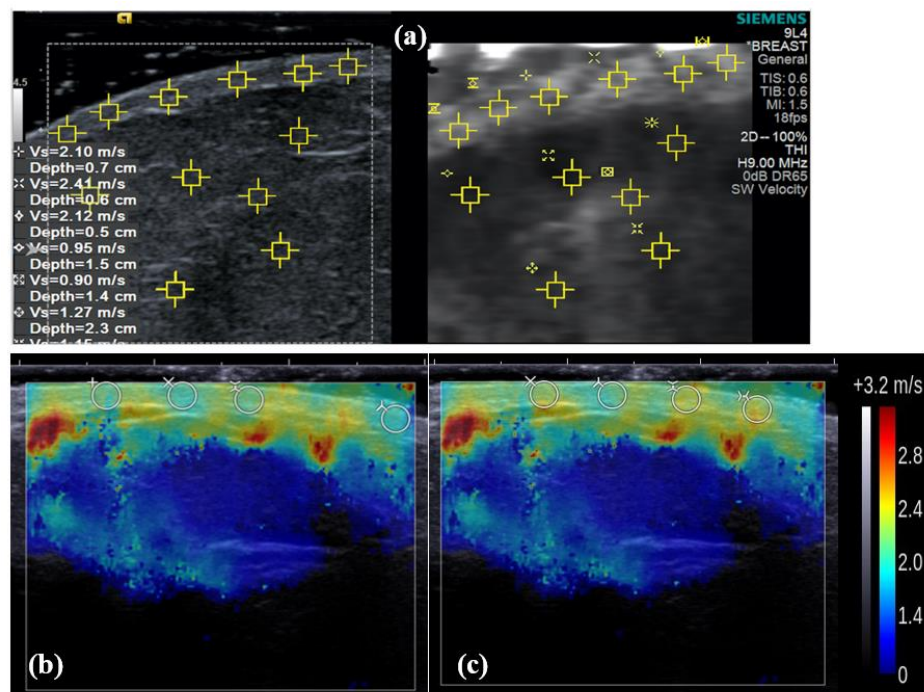

Figure 2. Showing: (**a**) An example B-mode image/elastogram pair acquired using the S2000 with ROIs marked on skin and parenchyma tissues (Volunteer 2); (**b**) an Aixplorer elastogram containing artefacts, overlaid with transparency on a B-mode image (Volunteer 2). In this example, c_s values were estimated by placing ROIs (Q-boxes) in the regions free from artefacts; (**c**) the same image where the ROIs were positioned without knowledge of the position of the artefacts, achieved by reducing the opacity of the displayed elastogram to zero. Note that the Aixplorer only displays the last 4 ROIs selected.

The Aixplorer provided an elastogram superimposed on the B-mode image where red and blue indicated greater and lesser c_s, respectively, as shown in Figure 2b. The smallest available ROI, 2 mm in diameter, was placed at six different locations on the skin, adipose and parenchyma, respectively. The anatomical regions of interest and the c_s measurement points selected by the radiologist and annotated on S2000 images were used to guide the placement of the ROIs on Aixplorer elastograms, which was performed by EH.

Image artefacts of high c_s at regularly spaced intervals were observed in Aixplorer elastograms. These are visible as a regular pattern of greater shear wave speed in Figure 2b and as vertical lines of greater shear wave speed illustrated using an elastogram of a homogenous region of the phantom in Figure 3a. To study the effect of this artefact, the Aixplorer analysis was performed twice, once by choosing measurement locations that avoided the artefacts using both the B-mode image and the elastogram to position the ROIs, as in Figure 2b, and once with measurement locations selected using only the B-mode image by increasing the c_s scale and reducing the opacity of the on-screen display of the elastogram to zero (see Figure 2c). In some elastograms, it was not possible to avoid some overlap of ROIs with regions that appeared to contain artefacts. In some cases, minimising the inclusion of artefacts reduced the number of measurement positions available. The number of c_s estimates obtained using the Aixplorer when avoiding artefacts varied between two and six.
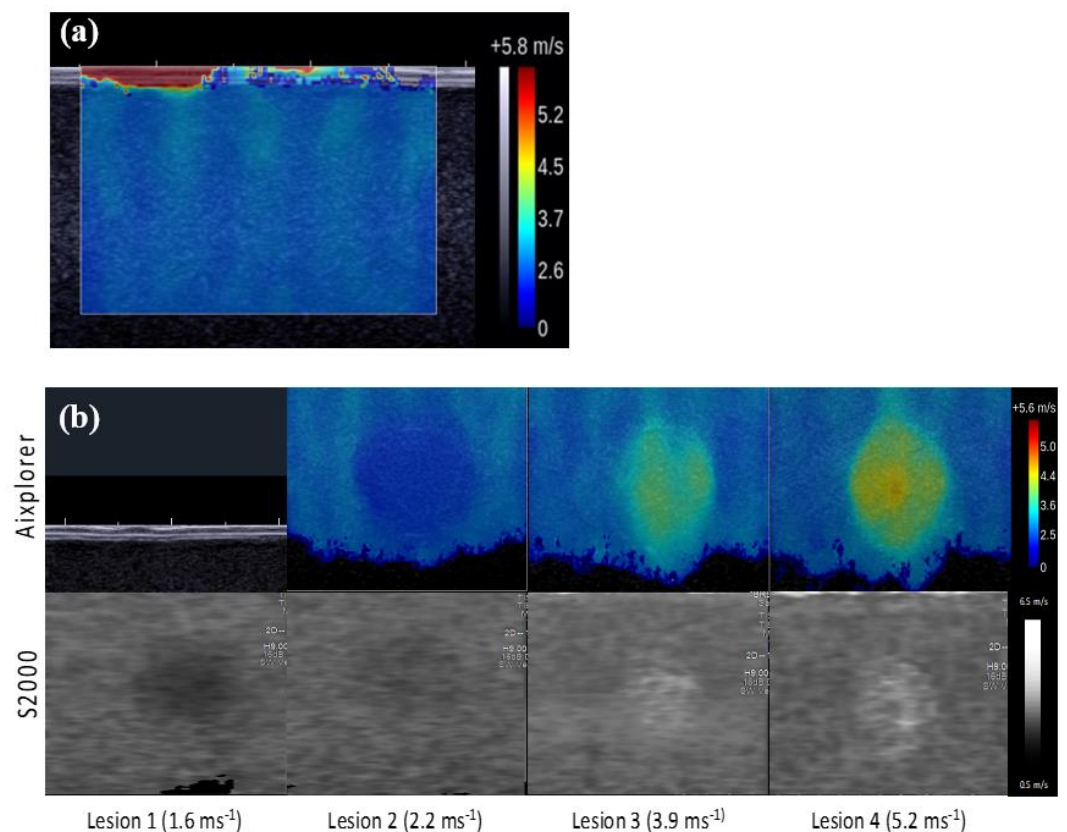

Figure 3. Showing: (**a**) Aixplorer image of a homogenous region of the phantom to illustrate the bands of greater shear wave speed (artefacts) observed. (**b**) Example elastograms of the lesions contained within the CIRS 049 phantom using the Aixplorer and the S2000. Nominal shear-wave speeds are given below the images.

2.5. Data Analysis

When analysing data from the elastography phantom, the agreement between machines was assessed using the percentage difference between c_s estimates measured using the Aixplorer and using the S2000. The symmetric percentage difference was defined

as the difference between estimates divided by the mean of the estimates multiplied by 100 [32] and are reported relative to Aixplorer values, i.e., a positive value indicates that the Aixplorer c_s estimate was greater than the S2000 c_s estimate. There were three values of percentage differences in c_s, one per observer. Interobserver variability of the c_s estimates for each inclusion and the background was quantified using the coefficient of variation (CV).

For each *in vivo* elastogram, mean c_s estimate were determined across all measurement locations (up to 6). Median, interquartile range (IQR), maximum and minimum values of these mean c_s estimates were determined for all breasts, for radial and anti-radial transducer orientations and for skin, adipose and parenchyma, and for individual subjects. For the Aixplorer this was done twice, including and excluding artefacts. Agreement between machine estimates of c_s was assessed using symmetric percentage differences in c_s estimates for each of the variables described above. The correlation between c_s estimates measured using S2000 and Aixplorer was determined using Pearson's correlation coefficient. In addition, the ability of the two machines to record the same contrast in mean c_s between the skin, adipose and parenchyma tissues was determined using tissue c_s ratios: skin to parenchyma, skin to adipose and adipose to parenchyma. Anisotropy of c_s was assessed per breast quadrant using the ratio of the mean c_s estimated from the anti-radial elastogram to that estimated from the corresponding radial elastogram.

Statistical analysis was performed with MatLab software (Version 2017a, The Mathworks Inc., Natick, MA, USA). Kolmogorov–Smirnov tests were used to test for normality. Wilcoxon signed-rank tests were used to perform a pair-wise analysis to test for agreement in median of the mean c_s estimates, tissue c_s ratios, and anisotropy ratios, between the machines. Pair-wise analysis was also performed to test for agreement between mean c_s estimates obtained using different transducer orientations in the skin, adipose and parenchyma.

3. Results

3.1. Difference in c_s Estimates between Machines In Vitro

Representative images of the phantom inclusions acquired using both machines are shown in Figure 3b. Table 1 lists the c_s estimates in the phantom measured by each observer, symmetric percentage differences c_s estimates in between machines, and the nominal values provided by the phantom manufacturer. Aixplorer gave between 0.2% to 3.06% greater c_s estimates than the S2000. The CVs of the c_s estimates were <0.1 for all regions of the phantom and both machines (see Table 1). Figure 2 shows example images of the lesions contained in the phantom acquired using both machines

Table 1. Individual and mean shear-wave speed (c_s) estimates from the Aixplorer and the S2000 and the coefficient of variation (CV) of c_s estimates across three observers. Individual estimates were the mean of three repeat measurements. The means and standard deviations of the symmetric percentage differences are given for each observer in the last column. The manufacturer's nominal c_s values for background and inclusions are given.

	Background	Inclusion 1	Inclusion 2	Inclusion 3	Inclusion 4	Mean (SD)
Nominal c_s	2.90	1.60	2.20	3.90	5.20	
Aixplorer: c_s estimates (ms^{-1})						
Observer 1	2.50	2.00	2.60	3.80	4.10	
Observer 2	2.60	1.90	2.50	3.70	4.30	
Observer 3	2.50	1.80	2.50	3.60	4.10	
Mean	2.53	1.90	2.53	3.70	4.17	
CV	0.02	0.05	0.02	0.03	0.03	

Table 1. *Cont.*

	Background	Inclusion 1	Inclusion 2	Inclusion 3	Inclusion 4	Mean (SD)
S2000: c_s estimates (ms^{-1})						
Observer 1	2.55	1.78	2.50	3.51	4.17	
Observer 2	2.47	1.89	2.40	3.40	4.11	
Observer 3	2.55	1.90	2.49	3.53	4.11	
Mean	2.50	1.90	2.50	3.50	4.10	
CV	0.02	0.04	0.02	0.02	0.01	
Symmetric percentage differences in c_s estimates (%)						
Observer 1	−0.99	5.82	1.96	3.97	−0.85	1.98 (2.98)
Observer 2	2.56	0.26	2.04	4.23	2.26	2.27 (1.41)
Observer 3	−0.99	−2.70	0.20	0.98	−0.12	−0.53 (1.41)
Mean	0.20	1.15	1.40	3.06	0.44	1.25 (1.12)

3.2. Difference in c_s Estimates between Machines In Vivo

A total of 128 elastograms were acquired, 64 for each machine. Ultrasound imaging revealed that one volunteer had small dense breasts comprising of mainly parenchymal tissue, this volunteer had a maximum imaging depth (skin to pectoral muscles) of approximately 2 cm. The other three volunteers had breasts of various sizes with differing amounts of adipose and parenchymal tissues, the maximum imaging depths in these volunteers were greater than 4 cm. Artefacts of ill-defined vertical bands of higher c_s than the average, appearing at approximately regularly spaced lateral intervals (as in Figure 3a, were observed in 100% of Aixplorer elastograms. In two Aixplorer images, artefacts covered the entire skin and adipose regions, and c_s estimates from regions without artefacts could not be obtained. In five Aixplorer elastograms, the elastogram-overlay box was incorrectly positioned below the outermost layer of the skin and c_s in the skin could not be obtained. A gel stand-off was clearly visualised on 96% of Aixplorer images and 100% of S2000 images. In two volunteers, the B-mode image did not clearly differentiate adipose tissue from the parenchyma. In these volunteers, c_s estimates were obtained in skin and parenchyma only.

Figure 4a illustrates that shear-wave speed estimates were significantly greater when measured using Aixplorer (avoiding artefacts) compared to S2000 in all tissue types (*p*-values < 0.001). Symmetric percentage differences in median c_s estimates between machines were 40.0%, 50.0% and 51.4% for skin, adipose and parenchyma tissues, respectively. The variance of Aixplorer mean c_s estimates was also statistically significantly greater than the variance of S2000 estimates (*p*-values < 0.001) in all tissues. The median and IQR of the mean c_s estimates were significantly less when measured excluding artefacts in the skin and adipose (*p*-values < 0.001) and gave better agreement with S2000 c_s estimates. All subsequent Aixplorer data presented were determined using c_s estimates measured avoiding artefacts. Pearson correlation coefficients between c_s estimates measured using individual elastograms acquired using S2000 and Aixplorer in the skin, adipose and parenchyma were 0.25, 0.15 and 0.33 and were not statistically significant (*p* > 0.05). When c_s estimates were averaged over the whole breast (eight elastograms) Pearson correlation coefficients were 0.16 (*p* = 0.5), 0.75 (*p* = 0.057) and 0.75 (*p* << 0.01), respectively. All data are tabulated in Table 2.
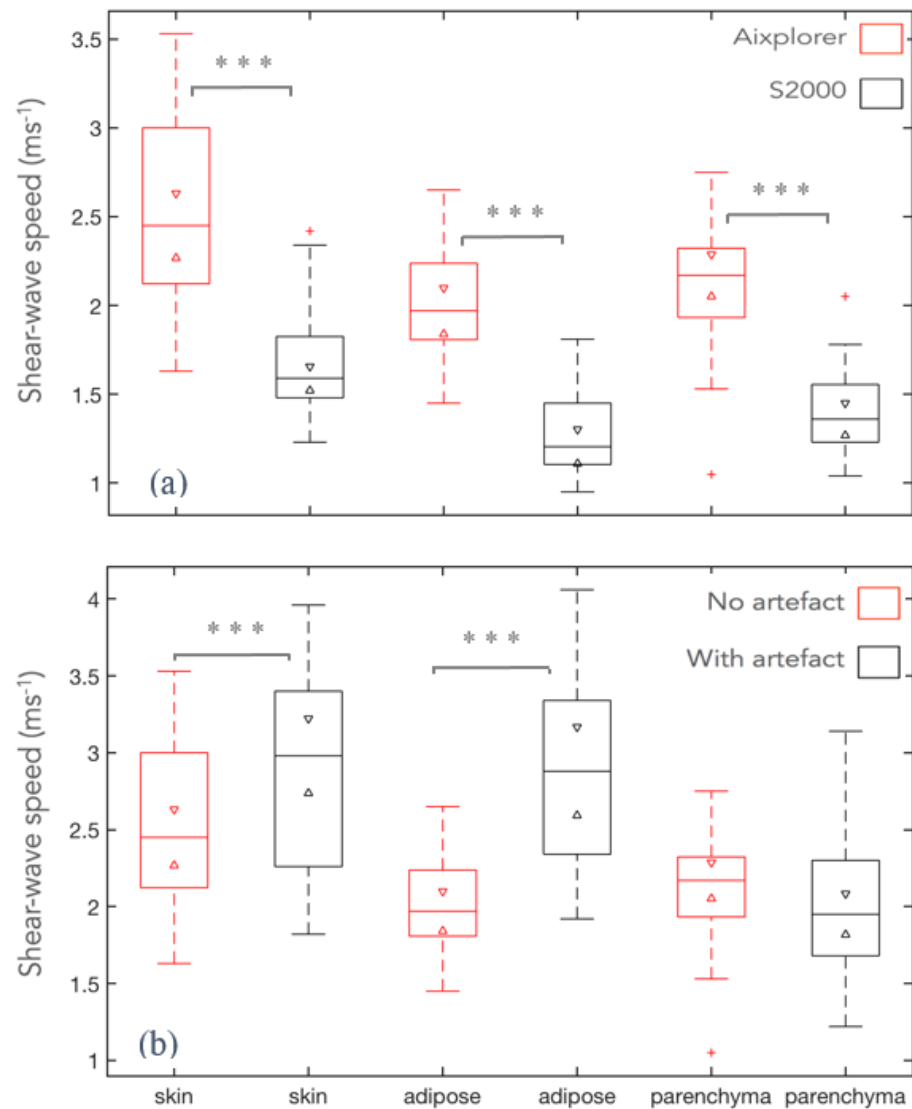
Figure 4. Showing: (**a**) Shear-wave speed (c_s) estimates for skin, adipose and parenchyma using Aixplorer (excluding artefacts) and S2000, and; (**b**) c_s estimates for skin, adipose and parenchyma measured using Aixplorer including and excluding artefacts. Median is illustrated by the central horizontal bar; the horizontal box edges show the IQR and the whiskers (dashed lines) show the range. Range is defined by adjacent values, which are the 25th or 75th quartile plus or minus the IQR multiplied by 1.5. Opposing triangles illustrate the 95% confidence interval on the median c_s and '+' indicates an outlier (any value outside the adjacent values). *** indicates where machine c_s estimates were significantly different with *p*-value < 0.001.

Table 2. Median, Interquartile range (IQR) max and mean shear-wave speed (c_s) estimates from the Aixplorer and the S2000 across all elastograms measured in skin adipose and parenchyma. S = skin, A = adipose and P = parenchyma.

	Mean c_s Estimate Per Elastogram (ms^{-1})								
	Aixplorer			**Aixplorer (with Artefacts)**			**S2000**		
	S	A	P	S	A	P	S	A	P
Median	2.4	2.0	2.2	3.0	2.9	3.0	1.6	1.2	1.3
IQR	0.9	0.4	0.6	0.9	0.4	0.6	0.3	0.3	0.3
Max	3.5	2.7	2.8	4.0	4.1	3.2	2.4	1.8	2.1
Min	1.6	1.5	1.2	1.8	1.9	1.2	1.2	1.0	1.0

3.3. Comparison of Tissue c_s Ratios between Machines

Figure 5 provides a box and whiskers plot of tissue c_s ratios per elastogram for both machines. For both machines, all median tissue c_s ratios were statistically significantly greater than unity, indicating that, on average, the skin had greater c_s than parenchyma and adipose tissues, and parenchyma had greater c_s than adipose tissue. There was no statistically significant difference in median tissue c_s ratios between machines.
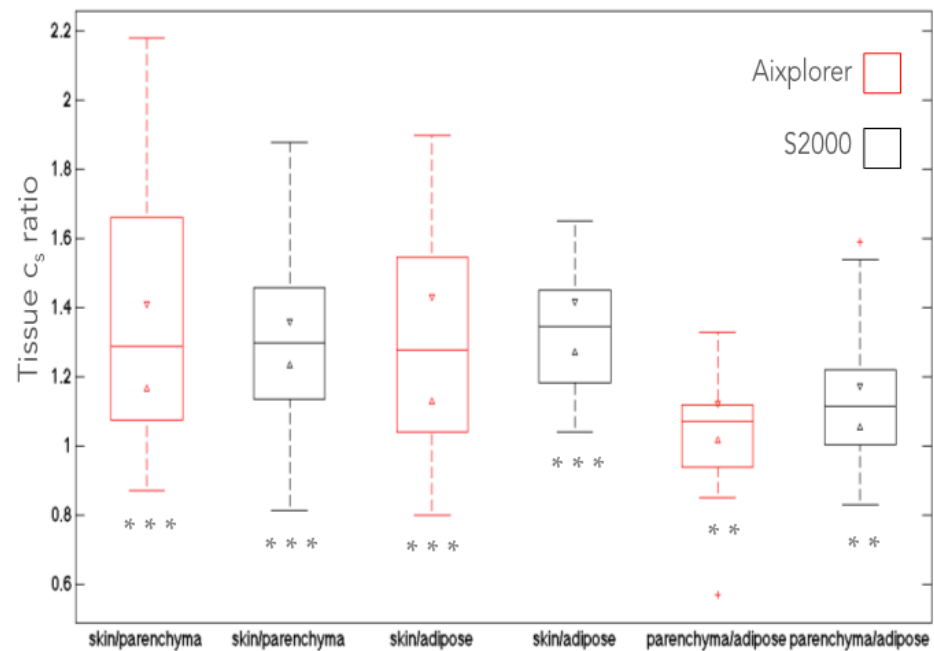

Figure 5. Tissue c_s ratios measured in skin, adipose and parenchyma in individual elastograms of the breast using Aixplorer and S2000. (See Figure 2 caption for full explanation of box plot). Aixplorer data were acquired using ROIs that did not include artefacts. The IQR and range may be influenced by variation between volunteers, breast quadrants and transducer orientation. ** or *** indicates where median c_s estimates for different tissue types were significantly different with *p*-value < 0.01 or < 0.001, respectively.

3.4. Comparison of Anisotropy Ratios between Machines

Figure 6 gives the median, IQR and range of anisotropy ratios for individual breast quadrants. Mean c_s estimates (per elastogram) were statistically significantly greater when the transducer was placed in an anti-radial orientation for all tissues and both machines except for estimates measured using Aixplorer in skin. When c_s estimates were averaged over the whole breast for anti-radial and radial positions, only for the S2000 did anti-radial c_s estimates remained statistically significantly higher than radial c_s estimates.
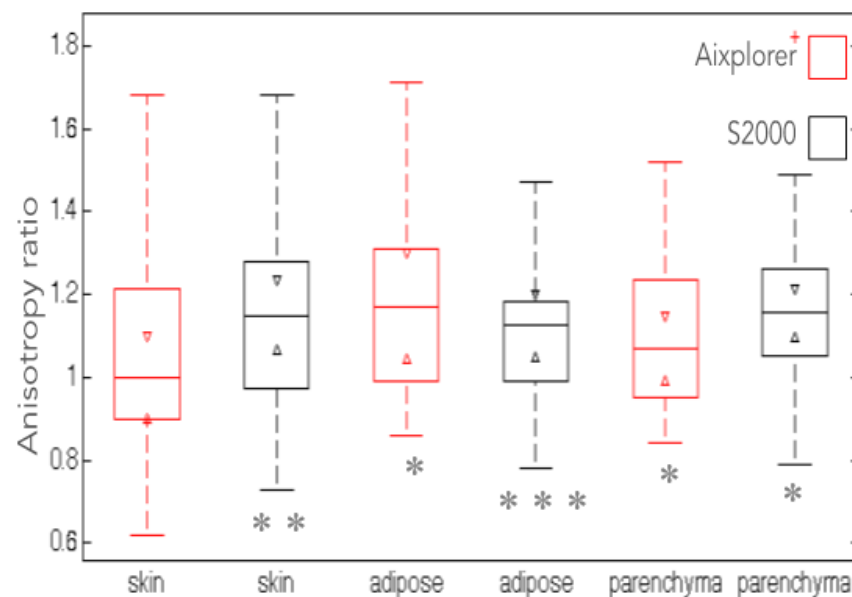
Figure 6. Anisotropy ratios (ratio of mean anti-radial c_s to mean radial c_s in individual pairs of elastograms obtained at the same location in the same breast quadrant on the same breast in the same individual) measured in skin, adipose and parenchyma for Aixplorer and S2000. *, ** or *** indicates where median c_s estimates for anti-radial and radial transducer orientations were significantly different with *p*-value < 0.05, < 0.01 or < 0.001, respectively.

4. Discussion

4.1. Difference in c_s Estimates between Machines In Vitro

Two studies have compared Siemens S2000 (or S3000) point SWE (pSWE) or 2D-SWE and Aixplorer c_s estimates *in vitro* using the same transducers that were used in the current study [15,18]. Using a phantom with nominal $c_s \approx 2.3 \text{ ms}^{-1}$ Shin et al. [15] found S2000 pSWE gave statistically significantly lower c_s estimates than Aixplorer by 0.1 ms^{-1} and 0.4 ms^{-1} at depths of 3.0 cm and 4.0 cm, respectively. Dillman et al. [18] compared S3000 pSWE with S3000 2D-SWE and Aixplorer 2D-SWE, at depths of 1.0, 2.5 and 4.0 cm in soft ($c_s \approx 0.9 \text{ ms}^{-1}$) and hard ($c_s \approx 2.1 \text{ ms}^{-1}$) phantoms and found small (<0.2 ms^{-1}) statistically significant differences between them, however, no consistent bias between machines was observed.

Hall [14] compared S2000 pSWE and Aixplorer 2D-SWE using curvilinear transducers at depths of 3.0, 4.5 and 7.0 cm across multiple machines at multiple sites. The Aixplorer gave significantly greater c_s estimates than the S2000, by up to ~0.2 ms^{-1} in a soft phantom ($c_s \approx 1.0 \text{ ms}^{-1}$). However, the use of a phased array transducer with the S2000 at one of the test sites may have biased the results; the S2000 c_s estimates at that site were significantly lower than the S2000 estimates at the other 4 sites. There was no statistically significant difference between the two machines in mean c_s estimates in a harder phantom ($c_s \approx 2.1 \text{ ms}^{-1}$). Similar to the above studies, the phantom data obtained in this study revealed only small differences in c_s between the machines, which were on the order of the interobserver variation. Estimates were obtained at a depth of 1.5 cm using linear transducers for both systems and therefore no bias due to depth or transducer geometry was expected.

4.2. Rationale for the Exclusion of Artefacts from Aixplorer Elastogram Analysis

All Aixplorer shear-wave elastograms obtained *in vivo* contained artefacts that appeared to correspond with the position of the acoustic radiation force beams; they moved with the lateral translation of the transducer and their number varied with the lateral size of the elastogram box. Artefacts were also observed *in vitro* and were most clearly visualised in the two stiffer inclusions. Across all volunteers, Aixplorer c_s estimates (including

artefacts) in adipose tissues were significantly greater than c_s estimates in parenchyma (Figure 4b, which was contrary to what has been reported in the literature. When artefacts were excluded the findings of the current study agreed with three large (minimum number of women 89) clinical studies that measured c_s in normal breast tissue using S2000 2D-SWE and found that breast parenchyma had statistically greater c_s than adipose tissue [26–28]. In addition, Athanasiou et al. [33] found similar results using Aixplorer in 46 women.

On visual examination of the elastograms, artefacts appeared most intense (greater c_s) below the gel-skin and skin-adipose interfaces. 'Artefactual vertical bands of stiffness' were observed by Berg et al. [34] in their study of breast lesions using Aixplorer 2D-SWE. Berg et al. [34] attributed these artefacts to tissue compression and noted they were difficult to avoid at superficial depths despite using large amounts of ultrasonic gel and a no-compression scanning protocol. We concluded that c_s estimates obtained in regions with artefacts were less reliable and only data from regions that were free from artefacts were used for subsequent analysis of anisotropy ratios.

4.3. Difference in c_s Estimates between Machines In Vivo

This study found that *in vivo*, S2000 c_s estimates were on average less than c_s estimates obtained using the Aixplorer. The differences between machines were greater *in vivo* than *in vitro*, with a maximum cross-machine c_s-ratio of 1.70 *in vivo* compared to 1.07 *in vitro*. To the authors' knowledge, this is the first study comparing c_s estimates of different elastography machines in the normal breast *in vivo*. Furthermore, c_s estimates between machines were uncorrelated except for c_s estimates for parenchyma averaged across the whole breast. The observed bias and poor correlation between machines exclude the use of an absolute measure of breast stiffness such as c_s or Young's Modulus, i.e., a simple value of breast stiffness would not be reproducible between centres. Further studies comparing these machines are required to determine if these biases can be corrected to provide consistent measures of breast tissue between centres. It is important to note that there were large differences in the variation between machines observed *in vitro* and *in vivo*. It appears from the data presented here that phantom studies would not be adequate to provide data for cross-calibrations of machines.

Several studies have compared liver c_s measured using 2D-SWE and pSWE *in vivo* [17,35–37] using a range of different commercially available pSWE and 2D-SWE machines and found that 2D-SWE and pSWE could not be used interchangeably to grade the severity of liver fibrosis in patients with liver disease. Ferraioli et al. [20] also compared two 2D-SWE machines (Aixplorer and Aplio 500 (Canon/Toshiba, Japan)) in 21 patients with liver disease. The mean difference between the two 2D SWE machines was -0.6 ms^{-1} and 95% LOA -1.4 ms^{-1} and 1.2 ms^{-1}; which of the machines gave the greatest c_s estimate was not reported.

Differences between c_s measured by different machines may, in part, be due to differences in the frequency content of the shear-waves. This would be consistent with our observation that such differences are greater for measurements in tissue than in phantoms since tissue is likely to possess increased shear wave dispersion due to viscoelastic damping or scattering of the shear wave relative to that in the phantom. Furthermore, it is possible that the way in which the ARFI pushing beams are executed, as described in the introduction, may result in different shear wave frequencies. Even with similar shear-wave bandwidth, if, to estimate c_s, vendors rely on a model of shear-wave propagation that assumes the spatial and temporal characteristics of the acoustic radiation force impulse (ARFI) push and the elastic or viscoelastic properties of the tissue, differences in models may result in differences in estimated c_s. It is also feasible that differences between machines arise due to differences in the ways in which their respective measurements of shear-wave speed are affected by the region within the lateral boundaries of the ARFI pushing beam, where a direct and immediate displacement from the ARFI push, whose magnitude decays with off-axis distance according to the ARFI intensity beam profile, is summed with the spatiotemporally varying displacement due to the propagating shear wave.

Further work is required to improve our understanding of the cause of machine bias and why it appears to be greater in tissue than in current phantoms. Nevertheless, even if standardisation of the frequency content of shear wave pulses used in SWE is not feasible, it would be helpful if manufacturers were able to provide the shear-wave frequency spectrum generated in typical tissues at a number of imaging depths, as part of the machine specification, so that authors could incorporate the information into publications such as this, as called for by Dietrich et al. [38].

4.4. Comparison of Tissue c_s Ratios and Anisotropy Ratios between Machines

For both machines, tissue c_s ratios were greater than unity indicating that skin had higher c_s estimates than parenchyma, and parenchyma had higher c_s estimates than adipose tissue. No significant differences in any tissue c_s ratios between machines were detected, suggesting that whilst the machines differed in absolute values of c_s estimates, relative values between tissue types are similar.

Zhou et al. [28] reported anisotropy ratios (radial to anti-radial) of 1.28 and 1.30 in adipose and parenchyma tissue in the normal breasts of 137 patients, respectively, measured using S2000 pSWE. These findings were consistent with the radial orientation of ducts and Cooper's ligaments and that material properties of the tissue are dependent on the orientation of tissue fibres. For example, Kruse et al. [39] and Gennisson et al. [40] in observations of muscle, and Coutts et al. [41] and Coutts et al. [42] in observations of skin, found that shear modulus and stiffness vary according to the direction of shear wave propagation and strain respectively, with respect to the muscle or dermal collagen fibres, and that c_s and stiffness were greatest when measured parallel to the fibres.

The current study detected a difference between c_s estimates measured in the radial and anti-radial orientations. The effect, however, was the reverse of that observed by Zhou et al. [28], with greater c_s measured with the transducer in the anti-radial orientation. The reason for this is unknown, although it may be significant that Zhou et al. [28] measured the c_s only at a single point with the probe in both orientations. The current study, which used a much smaller number of volunteers, compared average c_s across many measurement points in each image plane. The exact same volume of tissue was not being interrogated in each orientation, nor was the shear wave propagation direction truly anti-radial for any points other than at the central beamlines of the anti-radial scan, which may account for the different findings. For a direct comparison with the findings of Zhou et al., [28], a modification of our experimental method would be required, but this would be contrary to the objective of our study as discussed below.

The differences in c_s estimates between transducer orientations indicate that one or both transducer orientations should be used to acquire c_s estimates. Care should be taken to acquire data in the correct orientation, and perhaps this can be performed with reference to anatomical landmarks such as the nipple. The focus of the current study is the comparison of the machines for their ability to pool data, and the observed anisotropy in c_s estimates, although not consistent with the findings of Zhou et al. [28], was consistent between machines. This may suggest bias in the measurement technique, for example, a change in gel stand-off between the different transducer orientations, however, no systematic differences in gel stand-off between the images acquired using radial and ant-radial orientations was observed.

In the context of the future measurement of radiation toxicity to the breast and the use of the unirradiated breast as a reference measure of c_s, large variation in relative c_s estimates between normal breasts between machines would reduce the sensitivity of 2D-SWE to detect a change in stiffness in the breast due to radiation-induced fibrosis, i.e., any radiation-induced change in c_s, whether absolute or relative to the unirradiated breast, should be significantly greater than the equivalent natural variation in the population of women receiving radiotherapy for breast cancer. The magnitude of the effect of radiation on c_s in the tissues of the breast is as yet unknown. This cohort of volunteers is too small to investigate the underlying natural variation between breasts, however, we have

observed large variation in shear wave speeds between samples (Figure 4) and patients. Encouragement that it may be possible to use c_s for this purpose can be gained from the observations that semi-quantitative strain elastography using a calibrated stand-off pad demonstrated in all three of three patients who had received radiotherapy to the breast some years earlier, the irradiated breast had a higher Young's modulus that the unirradiated breast [43], and even subjective palpation is capable grading the level of breast stiffness changes that are caused by radiation damage and of distinguishing between the irradiated and unirradiated breast [1]. If the effect is smaller than the average variation between patients, it may be possible to use the contralateral breast as a reference or acquire a baseline (pre-treatment image) to measure the change in stiffness.

4.5. Limitations of This Study

A limitation of this study is the small number of volunteers. To compare SWE machines a cross-centre study had to be performed, which limited the number of volunteers available. Despite the small number of volunteers, differences in c_s estimates between machines were significant and consistent for all breasts and all tissue types. This study compared c_s estimates between machines in the skin. In skin, and othered layer tissue, such as the cornea, shear waves may be guided modifying the c_s and introducing dispersion [44] and the relationship between c_s and the elastic modulus can no longer be simply approximated by $E = 3\rho c_s^2$. Variation in the skin boundary conditions may also affect c_s [40]. Previous studies of 2D-SWE in skin have controlled for this effect. To investigate the relative stiffness of sclerotic and normal skin the relative c_s of sclerotic and normal skin was normalised by the ratio of skin thicknesses [45–47]. Similarly, in a study of the corneal collagen cross-linking using the Aixplorer, direct comparison of the stiffness of corneas with and without collagen cross-linking was justified by monitoring the central cornea thickness and ensuring there was no difference in cornea thickness between paired measurements [48]. In this work, cross-machine comparisons of c_s with the transducer in the same position on the breast were made and therefore skin thickness will be the same for both measurements. For future studies of radiation-induced breast toxicity using 2D-SWE, relative measures of radiation-induced skin toxicity that rely on comparison with the contralateral breast should consider variations in skin thickness and boundary conditions [45]. Another limitation is the use of a different operator to acquire *in vivo* data from each machine, which may introduce bias in c_s estimates. We also expect that interoperator variation may contribute to the poor correlation overserved between the elastograms acquired with different machines but of the same tissue sample. A further source of variation may be the placement of the probe on the breast, including changes in orientation. We used a surgical marker pen to mitigate against this variation, however, we expect that the heterogeneous nature of the breasts means that a small variation in probe placement could result in a small variation in c_s between scans. However, our use of two operators was by design, because it mimics the way that data would be acquired in a future multicentre study, it was expected that interoperator variation, which includes variations in probe placement, to be a small effect. Studies report good agreement between operators both *in vitro* and *in vivo* [14,19,20,37] and care was taken to give the two radiologists the same instructions and to allow them to practice data acquisition using a phantom.

5. Conclusions

Differences in c_s estimates between 2D-SWE machines were much greater *in vivo* than *in vitro*. Aixplorer gave a greater estimate of c_s than S2000 in all tissues. Differences in c_s estimates limit the use of absolute measures of c_s as a quantitative biomarker in cross-centre studies unless this bias can be reliably corrected. Shear-wave speed estimates must be acquired using the same transducer orientation across centres and across machines.

Author Contributions: Conceptualization, E.H., R.S., A.M.K. and J.C.B.; methodology, E.H., R.S. and J.C.B.; software; formal analysis, E.H.; investigation, E.H., E.O. and R.S.; data curation, E.H. writing—original draft preparation, E.H.; writing—review and editing, E.H., J.C.B., E.O., A.M.K. and

References

1. Haviland, J.S.; Owen, J.R.; Dewar, J.A.; Agrawal, R.K.; Barrett, J.; Barrett-Lee, P.J.; Dobbs, H.J.; Hopwood, P.; Lawton, P.A.; Magee, B.J.; et al. The uk standardisation of breast radiotherapy (start) trials of radiotherapy hypofractionation for treatment of early breast cancer: 10-year follow-up results of two randomised controlled trials. *Lancet Oncol.* **2013**, *14*, 1086–1094. [CrossRef]
2. Al-Ghazal, S.K.; Fallowfield, L.; Blamey, R.W. Does cosmetic outcome from treatment of primary breast cancer influence psychosocial morbidity? *Eur. J. Surg. Oncol.* **1999**, *25*, 571–573. [CrossRef]
3. Hoeller, U.; Tribius, S.; Kuhlmey, A.; Grader, K.; Fehlauer, F.; Alberti, W. Increasing the rate of late toxicity by changing the score? A comparison of rtog/eortc and lent/soma scores. *Int. J. Radiat. Oncol. Biol. Phys.* **2003**, *55*, 1013–1018. [CrossRef]
4. Taira, N.; Shimozuma, K.; Shiroiwa, T.; Ohsumi, S.; Kuroi, K.; Saji, S.; Saito, M.; Iha, S.; Watanabe, T.; Katsumata, N. Associations among baseline variables, treatment-related factors and health-related quality of life 2 years after breast cancer surgery. *Breast Cancer Res. Treat.* **2011**, *128*, 735–747. [CrossRef]
5. Mukesh, M.B.; Harris, E.; Collette, S.; Coles, C.E.; Bartelink, H.; Wilkinson, J.; Evans, P.M.; Graham, P.; Haviland, J.; Poortmans, P.; et al. Normal tissue complication probability (ntcp) parameters for breast fibrosis: Pooled results from two randomised trials. *Radiother. Oncol.* **2013**, *108*, 293–298. [CrossRef]
6. Andreassen, C.N.; Rosenstein, B.S.; Kerns, S.L.; Ostrer, H.; De Ruysscher, D.; Cesaretti, J.A.; Barnett, G.C.; Dunning, A.M.; Dorling, L.; West, C.M.L.; et al. Individual patient data meta-analysis shows a significant association between the atm rs1801516 snp and toxicity after radiotherapy in 5456 breast and prostate cancer patients. *Radiother. Oncol.* **2016**, *121*, 431–439. [CrossRef]
7. Barr, R.G.; Nakashima, K.; Amy, D.; Cosgrove, D.; Farrokh, A.; Schafer, F.; Bamber, J.C.; Castera, L.; Choi, B.I.; Chou, Y.H.; et al. Wfumb guidelines and recommendations for clinical use of ultrasound elastography: Part 2: Breast. *Ultrasound Med. Biol.* **2015**, *41*, 1148–1160. [CrossRef] [PubMed]
8. Evans, A.; Whelehan, P.; Thomson, K.; McLean, D.; Brauer, K.; Purdie, C.; Jordan, L.; Baker, L.; Thompson, A. Quantitative shear wave ultrasound elastography: Initial experience in solid breast masses. *Breast Cancer Res.* **2010**, *12*, R104. [CrossRef] [PubMed]
9. Shiina, T.; Nightingale, K.R.; Palmeri, M.L.; Hall, T.J.; Bamber, J.C.; Barr, R.G.; Castera, L.; Choi, B.I.; Chou, Y.H.; Cosgrove, D.; et al. Wfumb guidelines and recommendations for clinical use of ultrasound elastography: Part 1: Basic principles and terminology. *Ultrasound Med. Biol.* **2015**, *41*, 1126–1147. [CrossRef] [PubMed]
10. Rus, G.; Faris, I.H.; Torres, J.; Callejas, A.; Melchor, J. Why Are Viscosity and Nonlinearity Bound to Make an Impact in Clinical Elastographic Diagnosis? *Sensors* **2020**, *20*, 2379. [CrossRef]
11. Baues, M.; Dasgupta, A.; Ehling, J.; Prakash, J.; Boor, P.; Tacke, F.; Kiessling, F.; Lammers, T. Fibrosis imaging: Current concepts and future directions. *Adv. Drug Deliv. Rev.* **2017**, *121*, 9–26. [CrossRef] [PubMed]
12. Ajmera, V.; Loomba, R. Imaging biomarkers of NAFLD, NASH, and fibrosis. *Mol. Metab.* **2021**, *50*, 101167. [CrossRef] [PubMed]
13. Bamber, J.; Cosgrove, D.; Dietrich, C.F.; Fromageau, J.; Bojunga, J.; Calliada, F.; Cantisani, V.; Correas, J.M.; D'Onofrio, M.; Drakonaki, E.E.; et al. Efsumb guidelines and recommendations on the clinical use of ultrasound elastography. Part 1: Basic principles and technology. *Ultraschall Med.* **2013**, *34*, 169–184. [CrossRef] [PubMed]
14. Hall, T.J.; Milkowski, A.; Garra, B.; Carson, P.; Palmeri, M.; Nightingale, K.; Lynch, T.; Alturki, A.; Andre, M.; Audiere, S.; et al. Rsna/qiba: Shear wave speed as a biomarker for liver fibrosis staging. *IEEE Int. Ultrason Symp. IUS* **2013**, 397–400.
15. Shin, H.J.; Kim, M.J.; Kim, H.Y.; Roh, Y.H.; Lee, M.J. Comparison of shear wave velocities on ultrasound elastography between different machines, transducers, and acquisition depths: A phantom study. *Eur. Radiol.* **2016**, *26*, 3361–3367. [CrossRef] [PubMed]

16. Zhao, H.; Song, P.; Urban, M.W.; Kinnick, R.R.; Yin, M.; Greenleaf, J.F.; Chen, S. Bias observed in time-of-flight shear wave speed measurements using radiation force of a focused ultrasound beam. *Ultrasound Med. Biol.* **2011**, *37*, 1884–1892. [CrossRef] [PubMed]

17. Chang, S.; Kim, M.J.; Kim, J.; Lee, M.J. Variability of shear wave velocity using different frequencies in acoustic radiation force impulse (arfi) elastography: A phantom and normal liver study. *Ultraschall Med.* **2013**, *34*, 260–265. [CrossRef]

18. Dillman, J.R.; Chen, S.; Davenport, M.S.; Zhao, H.; Urban, M.W.; Song, P.; Watcharotone, K.; Carson, P.L. Superficial ultrasound shear wave speed measurements in soft and hard elasticity phantoms: Repeatability and reproducibility using two ultrasound systems. *Pediatr. Radiol.* **2015**, *45*, 376–385. [CrossRef]

19. Mulabecirovic, A.; Mjelle, A.B.; Gilja, O.H.; Vesterhus, M.; Havre, R.F. Repeatability of shear wave elastography in liver fibrosis phantoms-evaluation of five different systems. *PLoS ONE* **2018**, *13*, e0189671. [CrossRef]

20. Ferraioli, G.; De Silvestri, A.; Lissandrin, R.; Maiocchi, L.; Tinelli, C.; Filice, C.; Barr, R.G. Evaluation of inter-system variability in liver stiffness measurements. *Ultraschall Med.* **2019**, *40*, 64–75. [CrossRef]

21. Woo, H.; Lee, J.Y.; Yoon, J.H.; Kim, W.; Cho, B.; Choi, B.I. Comparison of the reliability of acoustic radiation force impulse imaging and supersonic shear imaging in measurement of liver stiffness. *Radiology* **2015**, *277*, 881–886. [CrossRef]

22. Huang, Y.P.; Zheng, Y.P.; Leung, S.F.; Choi, A.P. High frequency ultrasound assessment of skin fibrosis: Clinical results. *Ultrasound Med. Biol.* **2007**, *33*, 1191–1198. [CrossRef]

23. Liu, T.; Zhou, J.; Osterman, K.S.; Zhang, P.; Woodhouse, S.A.; Schiff, P.B.; Kutcher, G.J. Measurements of radiation-induced skin changes in breast-cancer radiation therapy using ultrasonic imaging. *Annu. Int. Conf. IEEE Eng. Med. Biol. Soc.* **2008**, *2*, 718–722.

24. Barnett, G.C.; Wilkinson, J.S.; Moody, A.M.; Wilson, C.B.; Twyman, N.; Wishart, G.C.; Burnet, N.G.; Coles, C.E. The cambridge breast intensity-modulated radiotherapy trial: Patient- and treatment-related factors that influence late toxicity. *Clin. Oncol.* **2011**, *23*, 662–673. [CrossRef] [PubMed]

25. Brierley, J.D.; Paterson, I.C.; Lallemand, R.C.; Rostom, A.Y. The influence of breast size on late radiation reaction following excision and radiotherapy for early breast cancer. *Clin. Oncol.* **1991**, *3*, 6–9. [CrossRef]

26. Golatta, M.; Schweitzer-Martin, M.; Harcos, A.; Schott, S.; Junkermann, H.; Rauch, G.; Sohn, C.; Heil, J. Normal breast tissue stiffness measured by a new ultrasound technique: Virtual touch tissue imaging quantification (vtiq). *Eur. J. Radiol.* **2013**, *82*, e676–e679. [CrossRef]

27. Wojcinski, S.; Brandhorst, K.; Sadigh, G.; Hillemanns, P.; Degenhardt, F. Acoustic radiation force impulse imaging with virtual touch tissue quantification: Mean shear wave velocity of malignant and benign breast masses. *Int. J. Womens Health* **2013**, *5*, 619–627. [CrossRef]

28. Zhou, J.; Yang, Z.; Zhan, W.; Dong, Y.; Zhou, C. Anisotropic properties of breast tissue measured by acoustic radiation force impulse quantification. *Ultrasound Med. Biol.* **2016**, *42*, 2372–2382. [CrossRef]

29. Friedrich-Rust, M.; Romenski, O.; Meyer, G.; Dauth, N.; Holzer, K.; Grünwald, F.; Kriener, S.; Herrmann, E.; Zeuzem, S.; Bojunga, J. Acoustic Radiation Force Impulse-Imaging for the evaluation of the thyroid gland: A limited patient feasibility study. *Ultrasonics* **2012**, *52*, 69–74. [CrossRef]

30. Tanter, M.; Bercoff, J.; Athanasiou, A.; Deffieux, T.; Gennisson, J.L.; Montaldo, G.; Muller, M.; Tardivon, A.; Fink, M. Quantitative assessment of breast lesion viscoelasticity: Initial clinical results using supersonic shear imaging. *Ultrasound Med. Biol.* **2008**, *34*, 1373–1386. [CrossRef] [PubMed]

31. Barr, R.G.; Zhang, Z. Effects of precompression on elasticity imaging of the breast: Development of a clinically useful semiquantitative method of precompression assessment. *J. Ultrasound Med.* **2012**, *31*, 895–902. [CrossRef]

32. Cole, T.J.; Altman, D.G. Statistics notes: What is a percentage difference? *BMJ* **2017**, *358*, j3663. [CrossRef]

33. Athanasiou, A.; Tardivon, A.; Tanter, M.; Sigal-Zafrani, B.; Bercoff, J.; Deffieux, T.; Gennisson, J.L.; Fink, M.; Neuenschwander, S. Breast lesions: Quantitative elastography with supersonic shear imaging–preliminary results. *Radiology* **2010**, *256*, 297–303. [CrossRef]

34. Berg, W.A.; Cosgrove, D.O.; Dore, C.J.; Schafer, F.K.; Svensson, W.E.; Hooley, R.J.; Ohlinger, R.; Mendelson, E.B.; Balu-Maestro, C.; Locatelli, M.; et al. Shear-wave elastography improves the specificity of breast us: The be1 multinational study of 939 masses. *Radiology* **2012**, *262*, 435–449. [CrossRef]

35. Fang, C.; Konstantatou, E.; Romanos, O.; Yusuf, G.T.; Quinlan, D.J.; Sidhu, P.S. Reproducibility of 2-dimensional shear wave elastography assessment of the liver: A direct comparison with point shear wave elastography in healthy volunteers. *J. Ultrasound Med.* **2017**, *36*, 1563–1569. [CrossRef]

36. Mulazzani, L.; Salvatore, V.; Ravaioli, F.; Allegretti, G.; Matassoni, F.; Granata, R.; Ferrarini, A.; Stefanescu, H.; Piscaglia, F. Point shear wave ultrasound elastography with esaote compared to real-time 2d shear wave elastography with supersonic imagine for the quantification of liver stiffness. *J. Ultrasound* **2017**, *20*, 213–225. [CrossRef]

37. Sigrist, R.M.S.; El Kaffas, A.; Jeffrey, R.B.; Rosenberg, J.; Willmann, J.K. Intra-individual comparison between 2-d shear wave elastography (ge system) and virtual touch tissue quantification (siemens system) in grading liver fibrosis. *Ultrasound Med. Biol.* **2017**, *43*, 2774–2782. [CrossRef] [PubMed]

38. Dietrich, C.F.; Bamber, J.; Berzigotti, A.; Bota, S.; Cantisani, V.; Castera, L.; Cosgrove, D.; Ferraioli, G.; Friedrich-Rust, M.; Gilja, O.H.; et al. Efsumb guidelines and recommendations on the clinical use of liver ultrasound elastography, update 2017 (long version). *Ultraschall Med.* **2017**, *38*, e16–e47. [PubMed]

39. Kruse, S.A.; Smith, J.A.; Lawrence, A.J.; Dresner, M.A.; Manduca, A.; Greenleaf, J.F.; Ehman, R.L. Tissue characterization using magnetic resonance elastography: Preliminary results. *Phys. Med. Biol.* **2000**, *45*, 1579–1590. [CrossRef] [PubMed]

40. Gennisson, J.L.; Deffieux, T.; Mace, E.; Montaldo, G.; Fink, M.; Tanter, M. Viscoelastic and anisotropic mechanical properties of in vivo muscle tissue assessed by supersonic shear imaging. *Ultrasound Med. Biol.* **2010**, *36*, 789–801. [CrossRef] [PubMed]

41. Coutts, L.V.; Bamber, J.; Miller, N.R.; Mortimer, P.S. Ultrasound elastography of the skin and subcutis under surface extensive loading. *Ultrasound* **2006**, *14*, 161–166. [CrossRef]

42. Coutts, L.V.; Miller, N.R.; Mortimer, P.S.; Bamber, J.C. Investigation of in vivo skin stiffness anisotropy in breast cancer related lymphoedema. *J. Biomech* **2016**, *49*, 94–99. [CrossRef] [PubMed]

43. Bush, N.L.; Bamber, J.C.; Barbone, P.; Yarnold, J.R. Semi-Quantitative Freehand Elastography for Assessing Radiation-Induced Breast Fibrosis. In Proceedings of the British Medical Ultrasound Society 37th Annual Scientific Meeting, Manchester, UK, 13–15 December 2005; Volume 13, p. 261.

44. Nguyen, T.M.; Couade, M.; Bercoff, J.; Tanter, M. Assessment of viscous and elastic properties of sub-wavelength layered soft tissues using shear wave spectroscopy: Theoretical framework and in vitro experimental validation. *IEEE Trans Ultrason Ferroelectr. Freq. Control.* **2011**, *58*, 2305–2315. [CrossRef]

45. Lee, S.Y.; Cardones, A.R.; Doherty, J.; Nightingale, K.; Palmeri, M. Preliminary results on the feasibility of using arfi/swei to assess cutaneous sclerotic diseases. *Ultrasound Med. Biol.* **2015**, *41*, 2806–2819. [CrossRef] [PubMed]

46. Wang, L.; Yan, F.; Yang, Y.; Xiang, X.; Qiu, L. Quantitative assessment of skin stiffness in localized scleroderma using ultrasound shear-wave elastography. *Ultrasound Med. Biol.* **2017**, *43*, 1339–1347. [CrossRef]

47. Yang, Y.; Qiu, L.; Wang, L.; Xiang, X.; Tang, Y.; Li, H.; Yan, F. Quantitative assessment of skin stiffness using ultrasound shear wave elastography in systemic sclerosis. *Ultrasound Med. Biol.* **2019**, *45*, 902–912. [CrossRef]

48. Touboul, D.; Gennisson, J.L.; Nguyen, T.M.; Robinet, A.; Roberts, C.J.; Tanter, M.; Grenier, N. Supersonic shear wave elastography for the in vivo evaluation of transepithelial corneal collagen cross-linking. *Investig. Ophthalmol. Vis. Sci.* **2014**, *55*, 1976–1984. [CrossRef] [PubMed]